Editors' Suggestion

Gate-Defined Topological Josephson Junctions in Bernal Bilayer Graphene

Ying-Ming Xie,[1,2,3] Étienne Lantagne-Hurtubise,[2,3] Andrea F. Young,[4] Stevan Nadj-Perge,[5,3] and Jason Alicea[2,3]
[1]Department of Physics, Hong Kong University of Science and Technology, Clear Water Bay, Hong Kong, China
[2]Department of Physics, California Institute of Technology, Pasadena, California 91125, USA
[3]Institute for Quantum Information and Matter, California Institute of Technology, Pasadena, California 91125, USA
[4]Department of Physics, University of California at Santa Barbara, Santa Barbara, California 93106, USA
[5]T. J. Watson Laboratory of Applied Physics, California Institute of Technology, 1200 East California Boulevard, Pasadena, California 91125, USA

(Received 28 April 2023; accepted 7 September 2023; published 5 October 2023)

Recent experiments on Bernal bilayer graphene (BLG) deposited on monolayer WSe_2 revealed robust, ultraclean superconductivity coexisting with sizable induced spin-orbit coupling. Here, we propose BLG/WSe_2 as a platform to engineer *gate-defined* planar topological Josephson junctions, where the normal and superconducting regions descend from a common material. More precisely, we show that if superconductivity in BLG/WSe_2 is gapped and emerges from a parent state with intervalley coherence, then Majorana zero-energy modes can form in the barrier region upon applying weak in-plane magnetic fields. Our results spotlight a potential pathway for "internally engineered" topological superconductivity that minimizes detrimental disorder and orbital-magnetic-field effects.

DOI: 10.1103/PhysRevLett.131.146601

Experimental searches for non-Abelian anyons have to date largely followed two complementary paths. The first seeks intrinsic realizations of strongly correlated topological phases of matter, most notably non-Abelian fractional quantum Hall states [1] and quantum spin liquids [2]. The second endeavors to engineer topological superconductors by interfacing well-understood building blocks—e.g., conventional superconductors and semiconductors—that originate from disparate materials [3–18]. One can, however, contemplate a middle ground between these strategies, wherein phases of matter intrinsic to a *single medium* are leveraged to "internally engineer" topological superconductivity. Graphene multilayers comprise an attractive platform for the latter approach given their extraordinarily rich and tunable phase diagrams. As proof of concept, Ref. [19] proposed that gate-defined wires judiciously immersed between gapped phases of twisted bilayer graphene [20–24], or its multilayer generalizations [25–29], could realize topological superconductivity without invoking "external" proximity effects (see also Refs. [30–33] for related architectures).

Untwisted (i.e., crystalline) graphene multilayers exhibit phase diagrams whose richness and tunability rival that of their twisted counterparts. Here, applying a perpendicular displacement field D opens a gap at charge neutrality and locally flattens the bands near the Brillouin zone corners—providing a knob to continuously tune the strength of electronic correlations. Experiments have reported a series of correlation-driven symmetry-broken metallic states together with superconductivity in both Bernal bilayer graphene (BLG) [34–39] and rhombohedral trilayer graphene [40,41], inspiring various theory proposals for the underlying pairing mechanism [42–58]. In BLG, superconductivity was first observed over a narrow density window in the presence of in-plane magnetic fields $B_{\parallel} \gtrsim 150$ mT, with a low critical temperature $T_c \approx 30$ mK [34]. More recent experiments [37,38] found that placing BLG adjacent to monolayer WSe_2 both generates appreciable spin-orbit coupling (SOC) *and* promotes Cooper pairing: Superconductivity appears over a broader density window within a symmetry-broken parent metallic phase, with T_c up to hundreds of mK, and without any applied magnetic field. Similar trends have now been observed in several graphene-based systems [23,37,59], suggesting a deep connection between SOC and enhanced pairing [50–52,60].

Here, we propose BLG/WSe_2 as a new platform for internally engineered topological superconductivity. Our proposal is inspired by seminal theory works [61,62] which showed that spin-orbit-coupled planar Josephson junctions at a phase difference of π can, in principle, host topological superconductivity at arbitrarily weak magnetic fields. Numerous experiments have since pursued this approach in junctions fashioned from proximitized heterostructures [63–67]. We show that Josephson junctions *generated solely by electrostatic gating* in BLG/WSe_2 [Fig. 1(a)] can similarly host a topological regime at weak magnetic fields, provided two requirements are satisfied: Superconductivity native to BLG/WSe_2 must exhibit a bulk gap [to ensure well-defined Andreev bound states (ABSs) in the junction] and descend from a symmetry-broken normal state with intervalley coherence (to lift valley degeneracy while maintaining the resonance

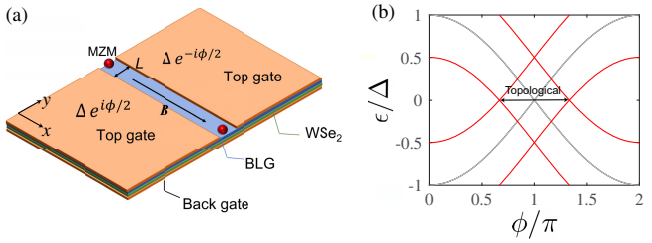

FIG. 1. (a) Gate-defined Josephson junction in BLG/WSe_2 predicted to host Majorana zero-energy modes (MZMs) near a phase difference $\phi = \pi$ with small in-plane magnetic fields $\boldsymbol{B}$. (b) Andreev bound states spectrum from Eq. (8) with Zeeman energy $\tilde{h} = 0$ (gray lines) and $\tilde{h} = 0.5\Delta$ (red lines), the latter opening a topological regime.

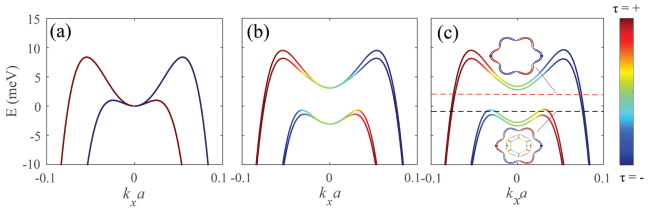

FIG. 2. Valence bands of BLG/WSe_2 at large displacement fields, calculated from Eq. (4) with $k_y = 0$ and $\lambda_1 = 0$. Parameters are (a) $\beta_I = \alpha_R = \lambda_0 = 0$ and (b),(c) $\beta_I = 1.4$ meV, $\alpha_R = 2$ meV $\cdot\, a$, and $\lambda_0 = 3$ meV; (c) further includes a Zeeman field $h = 0.3$ meV (along the x direction). Insets in (c) show the Fermi pockets arising with chemical potentials shown by the red and black dashed lines. Energy bands are colored according to their valley projection.

condition for intervalley Cooper pairing). At present, the superconducting order parameter and normal-state symmetry in BLG/WSe_2 remain unknown. Hartree-Fock treatments do, however, predict that various types of IVC states are energetically competitive in BLG [37,60], rhombohedral trilayer graphene [43,68–70], and twisted bilayer graphene [71–74] (see also a recent tensor-network study [75]). Moreover, IVC order was recently imaged using STM in monolayer graphene in its zeroth Landau level [76,77] as well as in twisted graphene bilayers [78] and trilayers [79]. Turning the problem on its head, one can view our proposal as a probe of IVC order in BLG/WSe_2.

Aside from eliminating the need for heterostructure engineering, our proposal entails two other key advantages: (i) Superconductivity in BLG/WSe_2 occurs deep in the clean limit [34,37], thereby mitigating adversarial disorder effects that remain a major obstruction in the pursuit of topological superconductivity, and (ii) the atomically thin nature of the setup reduces detrimental orbital effects of in-plane magnetic fields [67,80,81].

Symmetry-based low-energy description.—First, we derive a minimal effective Hamiltonian for the valence band of BLG/WSe_2 at large displacement fields D—where superconductivity emerges. As a baseline, Fig. 2(a) sketches the large-D valence band in the absence of SOC. The low-energy degrees of freedom carry spin and valley quantum numbers associated with Pauli matrices $s_{x,y,z}$ and $\tau_{x,y,z}$, respectively. The system preserves time-reversal symmetry $\mathcal{T} = i\tau_x s_y \mathcal{K}$ ($\mathcal{K}$ denotes complex conjugation) and threefold rotations $C_3 = e^{-i(\pi/3)s_z}$. We also impose the approximate $x \to -x$ mirror symmetry $M_x = i\tau_x s_x$, even though it is weakly broken by the WSe_2 substrate, and (for now) enforce valley conservation.

We express the single-particle Hamiltonian respecting these symmetries as

$$H_0(\boldsymbol{k}) = h_0(\boldsymbol{k}) + h_{\mathrm{so}}(\boldsymbol{k}), \tag{1}$$

where $\boldsymbol{k}$ denotes momentum measured with respect to the K and K' points. The first term captures the SOC-free band dispersion and can be decomposed as $h_0(\boldsymbol{k}) = \xi_0(\boldsymbol{k}) + \xi_1(\boldsymbol{k})\tau_z$. We take $\xi_0(\boldsymbol{k}) \approx -\mu + t_a\boldsymbol{k}^2 + t_c\boldsymbol{k}^4$ with μ the chemical potential; the valley-dependent contribution encodes trigonal warping and, to leading order in momentum, takes the form $\xi_1(\boldsymbol{k}) \approx t_b(k_x^3 - 3k_x k_y^2)$. By fitting to the full dispersion [82], we estimate $t_a = 4$ eV $\cdot\, a^2$, $t_b = -60$ eV $\cdot\, a^3$, and $t_c = -1500$ eV $\cdot\, a^4$, with $a = 0.246$ nm the lattice constant. The second term in Eq. (1) captures SOC in BLG inherited via virtual tunneling to WSe_2:

$$h_{\mathrm{so}}(\boldsymbol{k}) = \frac{\beta_I}{2}\tau_z s_z + \alpha_R(k_x s_y - k_y s_x). \tag{2}$$

Here, β_I and α_R, respectively, denote Ising and Rashba SOC couplings, whose magnitudes depend on the BLG/WSe_2 interface quality and twist angle [48,95–97]. For example, $\beta_I \sim 0.7$–2 meV was extracted using quantum Hall measurements in different devices [37,38,98]. The Rashba scale is harder to directly measure but can be conservatively estimated [82] as $\alpha_R \sim 1$–3 meV $\cdot\, a$.

Intervalley coherence.—Topological superconductivity emerges when an odd number of Fermi surfaces acquire a pairing gap. To this end, SOC in coordination with a Zeeman field facilitates the removal of spin degeneracy, though valley degeneracy in BLG provides an added obstruction. Coulomb interactions can lift the latter degeneracy by promoting symmetry breaking within the spin-valley subspace, akin to Stoner ferromagnetism [34–41]. Valley polarized states—in which electrons preferentially populate either the K or K' valley—are antagonistic to Cooper pairing and, thus, likely irrelevant for the parent state of superconductivity. We instead focus on IVC orders, wherein valley degeneracy is lifted via spontaneous coherent tunneling between K and K'; such states more naturally host superconductivity since the resonance condition for intervalley Cooper pairing can persist. Table I in Supplemental Material [82] classifies possible IVC orders. While we expect that our proposal holds for generic IVC

states, so long as they support gapped zero-momentum Cooper pairing, we focus for concreteness on the subset that preserves $\mathcal{T}$, C_3, and M_x. To linear order in momentum, the corresponding IVC order parameter can be expressed as

$$\Delta_{\mathrm{IVC}}(\boldsymbol{k}) = \lambda_0\tau_x + \lambda_1\tau_x(k_x s_y - k_y s_x), \tag{3}$$

where λ_0 describes a spin- and momentum-independent contribution and λ_1 encodes a spin-valley-orbit coupling.

Supplementing Eq. (1) with both the above IVC order parameter and an in-plane Zeeman field $\boldsymbol{h}$ yields the putative normal-state Hamiltonian

$$H(\boldsymbol{k}) = H_0(\boldsymbol{k}) + \Delta_{\mathrm{IVC}}(\boldsymbol{k}) + \boldsymbol{h}\cdot\boldsymbol{s} \tag{4}$$

that can exhibit fully lifted spin and valley degeneracies. Figures 2(b) and 2(c) sketch the band structure evolution upon (b) turning on SOC and IVC order and then (c) further adding a Zeeman field.

When the chemical potential intersects only the upper pair of bands [red dashed line in Fig. 2(c)], one can further distill the model by projecting out the lower, inert bands—yielding an effective Hamiltonian

$$\tilde{H}(\boldsymbol{k}) = \xi_0(\boldsymbol{k}) + \tilde{\beta}_I(k_x^3 - 3k_x k_y^2)\sigma_z + \tilde{\alpha}_R(k_x\sigma_y - k_y\sigma_x) + \tilde{\boldsymbol{h}}\cdot\boldsymbol{\sigma} \tag{5}$$

valid in the regime $h \ll \sqrt{\lambda_0^2 + \beta_I^2/4}$. Here, $\sigma_{x,y,z}$ are Pauli matrices acting in the low-energy subspace and

$$\tilde{\beta}_I = \frac{t_b\beta_I}{2\sqrt{\lambda_0^2 + \frac{\beta_I^2}{4}}}, \quad \tilde{\alpha}_R = \frac{\alpha_R\lambda_0}{\sqrt{\lambda_0^2 + \frac{\beta_I^2}{4}}} + \lambda_1, \quad \tilde{\boldsymbol{h}} = \frac{\boldsymbol{h}\lambda_0}{\sqrt{\lambda_0^2 + \frac{\beta_I^2}{4}}}. \tag{6}$$

Equation (5) represents a two-band model for fermions with cubic-in-momentum Ising SOC and linear-in-momentum Rashba SOC. Note that IVC order suppresses $\tilde{\beta}_I$ but enhances $\tilde{\alpha}_R$ and $\tilde{h}$ through a linear coupling to the bare Zeeman field h and Rashba SOC α_R, which only would be quadratic when $\lambda_0 = 0$. The spin-valley-orbit term λ_1 simply contributes to the effective Rashba coupling; we thus set $\lambda_1 = 0$ hereafter. Parameter renormalizations in Eq. (6) may be relevant for the unconventional Pauli-limit-violation trends observed in Ref. [37].

Topological Josephson junctions.—We now incorporate superconductivity, assuming for simplicity an s-wave order parameter—though we stress that our scheme readily extends to more exotic pairings provided they generate a bulk gap. The corresponding Bogoliubov–de Gennes (BdG) Hamiltonian reads

$$\tilde{H}_{\mathrm{BdG}}(\boldsymbol{k}) = \begin{pmatrix} \tilde{H}(\boldsymbol{k}) & i\Delta\sigma_y \\ -i\Delta\sigma_y & -\tilde{H}^*(-\boldsymbol{k}) \end{pmatrix} \tag{7}$$

with Δ the pairing amplitude. To set the stage, we first consider a simple case where $\xi_0(\boldsymbol{k}) \approx -\boldsymbol{k}^2/2m - \mu$ and $\tilde{\beta}_I k_F^3 \ll \tilde{\alpha}_R k_F$ (m is an effective mass and k_F is the Fermi momentum). Equation (7) then maps to the Hamiltonian for a proximitized Rashba-coupled 2D electron gas under in-plane magnetic fields—exactly the ingredients required to create topological superconductivity in planar Josephson junctions [61,62].

Next, we consider a Josephson junction, with phase difference ϕ, formed by gate tuning a barrier region of length L into a normal phase with $\Delta = 0$. The magnetic field is oriented parallel to the junction (along the x direction), which is optimal for accessing the topological regime [61,62]. Within the barrier, the relevant Fermi velocity v_F arises from the large pockets in Fig. 2(c); band-structure estimates give $v_F \sim 5 \times 10^5$ m/s. For reasonable junction lengths $L \sim 50$–200 nm, the corresponding Thouless energy $E_T = (\pi v_F/2L) \sim 0.8$–$3$ meV greatly exceeds both the pairing energy Δ and renormalized Zeeman energy $\tilde{h}$. We therefore assume the short-junction limit $E_T \gg \Delta, \tilde{h}$ below.

Topological phase transitions are determined by computing the ABS spectrum at $k_x = 0$ using the standard scattering matrix method (for details, see Supplemental Material [82]). In the absence of normal reflections at the interfaces, the $k_x = 0$ ABS energies take the simple form

$$\epsilon_{\pm,\eta}(\phi) = \eta\tilde{h} \pm \Delta\cos(\phi/2), \tag{8}$$

where $\eta = \pm$ is a pseudospin label. Figure 1(b) plots these energies at $\tilde{h} = 0$ and $\tilde{h} = 0.5\Delta$. In the zero-field limit, both $\eta = \pm$ branches become gapless at a phase difference $\phi = \pi$. Turning on the in-plane Zeeman field shifts the gap closing points to $\phi \neq \pi$, thereby opening up a topological regime. The above features are consistent with the results in Refs. [61,62], except that we consider a uniform Zeeman energy in the barrier and superconducting regions. The $\tilde{h}$ contribution in $\epsilon_{\pm,\eta}$ descends from the Zeeman energy in the superconductors—which produces nondegenerate $k_x = 0$ energies at $\phi = 0$.

Numerical phase diagram.—We now verify the above physical picture via a numerical calculation of the ABSs in a more realistic BLG/WSe_2 model. We rewrite the four-band Hamiltonian capturing the low-energy bands, Eqs. (4) and (7), as a tight-binding model in the y direction for a given k_x (see Supplemental Material, Sec. V [82]). To emulate experiments, where quantum oscillations reveal that superconductivity occurs in a regime with both large and small pockets [37], we fix the chemical potential in the superconducting regions to $\mu_2 = -1$ meV [black dashed line in Fig. 2(c)]. The chemical potential μ_1 in the barrier

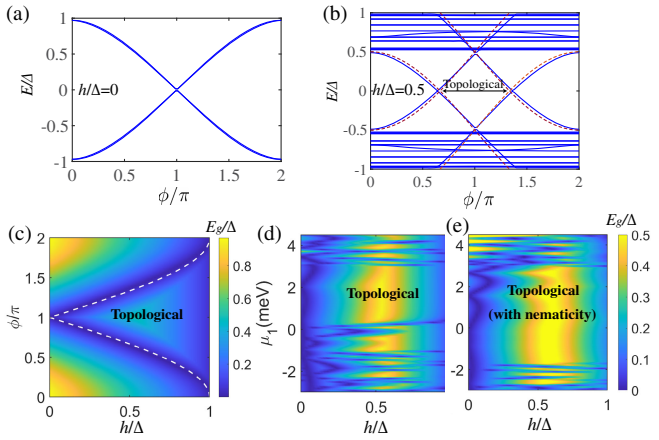

FIG. 3. (a),(b) ABS energies E at $k_x = 0$ as a function of ϕ, obtained from a realistic tight-binding model with Zeeman energy (a) $h = 0$ and (b) $h = 0.5\Delta$. Dashed lines in (b) trace the analytical result Eq. (8) obtained in the short junction limit. (c)–(e) Phase diagrams as a function of (c) h, ϕ and (d),(e) h, μ_1. In (c), the dashed white line indicates $h = \Delta|\cos(\phi/2)|$, which roughly captures the topological phase boundary. (e) is the same as (d) but with nematicity phenomenologically incorporated. Data correspond to $L = 158$ nm and $\phi = \pi$.

can be tuned independently, including to a regime with only large pockets (where the effective two-band model applies). For concreteness, unless specified otherwise we set $\mu_1 = 2$ meV, $\beta_I = 1.4$ meV, $\alpha_R = 2$ meV $\cdot a$, $\lambda_0 = 3$ meV, $\lambda_1 = 0$, and $\Delta = 0.1$ meV; under BCS weak-coupling assumptions, the latter corresponds to $T_c \sim 600$ mK. Note that this choice of λ_0 and β_I gives $\tilde{h} \approx h$.

The ABS spectrum follows by diagonalizing the 1D tight-binding model for each k_x. Figures 3(a) and 3(b) present the $k_x = 0$ energies versus ϕ for (a) $h = 0$ and (b) $h = 0.5\Delta$. In Fig. 3(a), lifting of valley degeneracy by IVC order leaves two nearly degenerate ABSs with a small splitting (away from $\phi = 0, \pi$). Figure 3(b) shows that a Zeeman field nucleates a topological region centered around $\phi = \pi$, separated from the trivial regions by a $k_x = 0$ gap closure. These observations agree well with simpler two-band-model results from Fig. 1(b); indeed, the bound states continue to be well captured by Eq. (8) [see dashed lines in Fig. 3(b)]. Figure 3(c) shows the broader phase diagram, obtained from the $k_x = 0$ gap (E_g) illustrated by the color map, versus h/Δ and ϕ. In the topological phase, the minimal gap $E_{g,m}$ typically appears at finite k_x and is maximized when SOC effects are dominated by the effective Rashba contribution (see Supplemental Material, Sec. VI [82]). The topological phase transition lines closely emulate the curves $\tilde{h} = \Delta|\cos(\phi/2)|$ predicted by Eq. (8). For the π junction, topological superconductivity sets in at arbitrarily weak Zeeman fields—though more generally normal reflections at the interfaces push the required Zeeman field to a finite value [61] (see Supplemental Material, Sec. III [82]). As the in-plane field increases, the topological phase persists until the superconducting regions become gapless, roughly when the renormalized Zeeman energy $\tilde{h} \sim \Delta$.

Figure 3(d) reveals the dependence of E_g on h/Δ and the barrier chemical potential μ_1 at $\phi = \pi$. A robust topological region occurs for $\mu_1 \sim 0$–3 meV, where the barrier hosts only two large hole pockets. Outside of this range, additional small pockets arise—see Fig. 2(c)—that engender frequent topological phase transitions. Quantum oscillations, however, indicate that the number of small pockets above T_c is smaller than the six naively predicted by band theory [37], which was suggested to arise from electronic nematicity [99,100]. Including nematicity in our calculation (see Supplemental Material, Sec. IV [82]), we find that the overall features of the phase diagram persist, while the extent of the robust topological region increases due to fewer "polluting" low-energy states.

Atomically resolved MZM wave functions.—Topological superconductivity acquires a novel fingerprint in our setup: The essential ingredient of IVC order generates atomic-scale translation symmetry breaking with an enlarged $\sqrt{3} \times \sqrt{3}$ Kekulé supercell, which manifests directly in the MZM wave functions. Figure 4(a) illustrates the atomically resolved MZM density of states in the barrier (see Supplemental Material [82], Sec. VIII); the usual exponential localization and Friedel-like oscillations are evident on the scale shown. Fourier transforming the data reveals characteristic momentum-space peaks [Fig. 4(b)] associated with the Kekulé supercell, while Fig. 4(c) enlarges the red rectangular region from (a) and clearly shows the corresponding atomic-scale ordering. Contrary

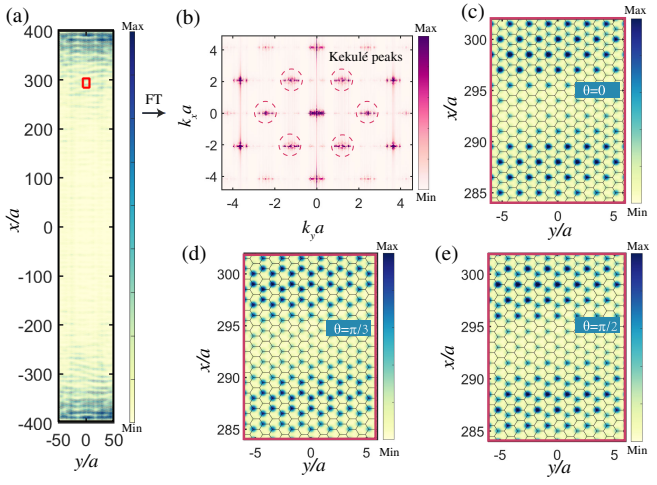

FIG. 4. (a) Atomically resolved density of states for the MZM wave function in the junction, assuming Kekulé angle $\theta = 0$. (b) Fourier transform (FT) of the data in (a) revealing Kekulé peaks resulting from IVC-induced atomic-scale reconstruction. (c)–(e) Enlargement of the red rectangular region in (a) showing the evolution of the symmetry-breaking pattern with different Kekulé angles. Data correspond to $L = 160a$, $h/\Delta = 0.8$, and $\phi = \pi$.

to the familiar "bond-centered" Kekulé patterns observed in monolayer graphene [76,77], here symmetry breaking manifests primarily on sites due to sublattice and layer polarization generated at large D fields. Figures 4(d) and 4(e) explore different Kekulé angles θ, obtained by replacing the τ_x order parameter considered thus far with $\cos(\theta)\tau_x + \sin(\theta)\tau_y$. The resulting Kekulé pattern intimately relates to θ, allowing experimental characterization of IVC order via the MZMs.

STM measurements that resolve zero-bias peaks without the atomic-scale structure predicted here could arise from trivial ABSs originating from disorder [101–103] or inhomogeneities near the barrier ends [104–106] (see Refs. [18,107] for reviews). Conversely, and more definitively, observing localized zero modes at both junction ends that appear near $\phi = \pi$ *and* exhibit Kekulé order would strongly support topological superconductivity arising from an IVC normal state.

Discussion and outlook.—We proposed a route to one-dimensional topological superconductivity where all required ingredients—SOC, Cooper pairing, and the ability to fabricate planar Josephson junctions—appear natively in a *single* BLG/WSe_2 platform. Our proposal relies on two reasonable but so far untested assumptions: a gapped superconducting phase and a normal parent state with intervalley coherence. The ultraclean nature of superconductivity in BLG [34,37], with an electronic mean-free path far exceeding the coherence length, presents an enormous virtue that potentially circumvents disorder effects that plague proximitized nanowires [101–103] and Josephson junctions [63–67]. Weak disorder arising, e.g., from imperfections in the geometry of gates defining the junction, can even enhance the robustness of the topological phase by decreasing the Majorana localization length [108]. A more controllable route to the same goal consists of gate defining the junction in a zigzag geometry designed to enhance Andreev reflections [109].

Our proposal readily generalizes to more exotic order parameters (see Supplemental Material, Table I [82]). If either the normal or superconducting state spontaneously breaks time-reversal symmetry, topological superconductivity could arise without an applied magnetic field [19]. For example, a spin-nematic IVC state described by a $\tau_x s_x$ order parameter generates an effective Zeeman field when projected to the low-energy subspace of Eq. (5). We also expect our proposal to be relevant for a broader family of graphene-based structures. Substantial efforts have been devoted to gate-defined wires and Josephson junctions in twisted bilayer graphene [19,30–33,110–112], which also enjoys exquisite gate tunability but suffers from more prevalent disorder [113,114]. Rhombohedral trilayer graphene offers a cleaner platform for gate-tunable correlated states and superconductivity [40,41]—thus presenting another interesting medium for future exploration along these lines.

We are grateful to Andrey Antipov, Cory Dean, Cyprian Lewandowski, Alex Thomson, and Yiran Zhang for enlightening discussions. Y.-M. X. acknowledges the support of Hong Kong Research Grant Council through PDFS2223-6S01. É. L.-H. was supported by the Gordon and Betty Moore Foundation's EPiQS Initiative, Grant No. GBMF8682. J. A. was supported by the Army Research Office under Grant No. W911NF-17-1-0323; the Caltech Institute for Quantum Information and Matter, an NSF Physics Frontiers Center with support of the Gordon and Betty Moore Foundation through Grant No. GBMF1250; and the Walter Burke Institute for Theoretical Physics at Caltech. The U.S. Department of Energy, Office of Science, National Quantum Information Science Research Centers, Quantum Science Center supported the symmetry-based analysis of this work. S. N.-P. acknowledges support of Office of Naval Research (Grant No. N142112635) and NSF-CAREER (DMR-1753306) programs. Work at UCSB was supported by the U.S. Department of Energy (Grant No. DE-SC0020305).

[1] C. Nayak, S. H. Simon, A. Stern, M. Freedman, and S. Das Sarma, Non-Abelian anyons and topological quantum computation, Rev. Mod. Phys. **80**, 1083 (2008).
[2] A. Kitaev, Anyons in an exactly solved model and beyond, Ann. Phys. (Amsterdam) **321**, 2 (2006).
[3] L. Fu and C. L. Kane, Superconducting Proximity Effect and Majorana Fermions at the Surface of a Topological Insulator, Phys. Rev. Lett. **100**, 096407 (2008).
[4] J. D. Sau, R. M. Lutchyn, S. Tewari, and S. Das Sarma, Generic New Platform for Topological Quantum Computation using Semiconductor Heterostructures, Phys. Rev. Lett. **104**, 040502 (2010).
[5] R. M. Lutchyn, J. D. Sau, and S. Das Sarma, Majorana Fermions and a Topological Phase Transition in Semiconductor-Superconductor Heterostructures, Phys. Rev. Lett. **105**, 077001 (2010).
[6] Y. Oreg, G. Refael, and F. von Oppen, Helical Liquids and Majorana Bound States in Quantum Wires, Phys. Rev. Lett. **105**, 177002 (2010).
[7] J. Alicea, Majorana fermions in a tunable semiconductor device, Phys. Rev. B **81**, 125318 (2010).
[8] V. Mourik, K. Zuo, S. M. Frolov, S. R. Plissard, E. P. A. M. Bakkers, and L. P. Kouwenhoven, Signatures of Majorana fermions in hybrid superconductor-semiconductor nanowire devices, Science **336**, 1003 (2012).
[9] T.-P. Choy, J. M. Edge, A. R. Akhmerov, and C. W. J. Beenakker, Majorana fermions emerging from magnetic nanoparticles on a superconductor without spin-orbit coupling, Phys. Rev. B **84**, 195442 (2011).
[10] S. Nadj-Perge, I. K. Drozdov, B. A. Bernevig, and A. Yazdani, Proposal for realizing Majorana fermions in chains of magnetic atoms on a superconductor, Phys. Rev. B **88**, 020407(R) (2013).
[11] F. Pientka, L. I. Glazman, and F. von Oppen, Topological superconducting phase in helical Shiba chains, Phys. Rev. B **88**, 155420 (2013).

[12] J. Klinovaja, P. Stano, A. Yazdani, and D. Loss, Topological Superconductivity and Majorana Fermions in RKKY Systems, Phys. Rev. Lett. **111**, 186805 (2013).
[13] S. Nadj-Perge, I. K. Drozdov, J. Li, H. Chen, S. Jeon, J. Seo, A. H. MacDonald, B. A. Bernevig, and A. Yazdani, Observation of Majorana fermions in ferromagnetic atomic chains on a superconductor, Science **346**, 602 (2014).
[14] X.-L. Qi and S.-C. Zhang, Topological insulators and superconductors, Rev. Mod. Phys. **83**, 1057 (2011).
[15] J. Alicea, New directions in the pursuit of Majorana fermions in solid state systems, Rep. Prog. Phys. **75**, 076501 (2012).
[16] C. Beenakker, Search for Majorana fermions in superconductors, Annu. Rev. Condens. Matter Phys. **4**, 113 (2013).
[17] R. M. Lutchyn, E. P. A. M. Bakkers, L. P. Kouwenhoven, P. Krogstrup, C. M. Marcus, and Y. Oreg, Majorana zero modes in superconductor–semiconductor heterostructures, Nat. Rev. Mater. **3**, 52 (2018).
[18] K. Flensberg, F. von Oppen, and A. Stern, Engineered platforms for topological superconductivity and Majorana zero modes, Nat. Rev. Mater. **6**, 944 (2021).
[19] A. Thomson, I. M. Sorensen, S. Nadj-Perge, and J. Alicea, Gate-defined wires in twisted bilayer graphene: From electrical detection of intervalley coherence to internally engineered Majorana modes, Phys. Rev. B **105**, L081405 (2022).
[20] Y. Cao, V. Fatemi, S. Fang, K. Watanabe, T. Taniguchi, E. Kaxiras, and P. Jarillo-Herrero, Unconventional superconductivity in magic-angle graphene superlattices, Nature (London) **556**, 43 (2018).
[21] M. Yankowitz, S. Chen, H. Polshyn, Y. Zhang, K. Watanabe, T. Taniguchi, D. Graf, A. F. Young, and C. R. Dean, Tuning superconductivity in twisted bilayer graphene, Science **363**, 1059 (2019).
[22] X. Lu, P. Stepanov, W. Yang, M. Xie, M. A. Aamir, I. Das, C. Urgell, K. Watanabe, T. Taniguchi, G. Zhang, A. Bachtold, A. H. MacDonald, and D. K. Efetov, Superconductors, orbital magnets and correlated states in magic-angle bilayer graphene, Nature (London) **574**, 653 (2019).
[23] H. S. Arora, R. Polski, Y. Zhang, A. Thomson, Y. Choi, H. Kim, Z. Lin, I. Z. Wilson, X. Xu, J.-H. Chu, K. Watanabe, T. Taniguchi, J. Alicea, and S. Nadj-Perge, Superconductivity in metallic twisted bilayer graphene stabilized by WSe2, Nature (London) **583**, 379 (2020).
[24] M. Oh, K. P. Nuckolls, D. Wong, R. L. Lee, X. Liu, K. Watanabe, T. Taniguchi, and A. Yazdani, Evidence for unconventional superconductivity in twisted bilayer graphene, Nature (London) **600**, 240 (2021).
[25] J. M. Park, Y. Cao, K. Watanabe, T. Taniguchi, and P. Jarillo-Herrero, Tunable strongly coupled superconductivity in magic-angle twisted trilayer graphene, Nature (London) **590**, 249 (2021).
[26] Z. Hao, A. M. Zimmerman, P. Ledwith, E. Khalaf, D. H. Najafabadi, K. Watanabe, T. Taniguchi, A. Vishwanath, and P. Kim, Electric field tunable superconductivity in alternating-twist magic-angle trilayer graphene, Science **371**, 1133 (2021).
[27] H. Kim, Y. Choi, C. Lewandowski, A. Thomson, Y. Zhang, R. Polski, K. Watanabe, T. Taniguchi, J. Alicea, and S. Nadj-Perge, Evidence for unconventional superconductivity in twisted trilayer graphene, Nature (London) **606**, 494 (2022).
[28] J. M. Park, Y. Cao, L.-Q. Xia, S. Sun, K. Watanabe, T. Taniguchi, and P. Jarillo-Herrero, Robust superconductivity in magic-angle multilayer graphene family, Nat. Mater. **21**, 877 (2022).
[29] Y. Zhang, R. Polski, C. Lewandowski, A. Thomson, Y. Peng, Y. Choi, H. Kim, K. Watanabe, T. Taniguchi, J. Alicea, F. von Oppen, G. Refael, and S. Nadj-Perge, Promotion of superconductivity in magic-angle graphene multilayers, Science **377**, 1538 (2022).
[30] D. Rodan-Legrain, Y. Cao, J. M. Park, S. C. de la Barrera, M. T. Randeria, K. Watanabe, T. Taniguchi, and P. Jarillo-Herrero, Highly tunable junctions and non-local Josephson effect in magic-angle graphene tunnelling devices, Nat. Nanotechnol. **16**, 769 (2021).
[31] F. K. de Vries, E. Portolés, G. Zheng, T. Taniguchi, K. Watanabe, T. Ihn, K. Ensslin, and P. Rickhaus, Gate-defined Josephson junctions in magic-angle twisted bilayer graphene, Nat. Nanotechnol. **16**, 760 (2021).
[32] E. Portolés, S. Iwakiri, G. Zheng, P. Rickhaus, T. Taniguchi, K. Watanabe, T. Ihn, K. Ensslin, and F. K. de Vries, A tunable monolithic squid in twisted bilayer graphene, Nat. Nanotechnol. **17**, 1159 (2022).
[33] J. Díez-Mérida, A. Díez-Carlón, S. Y. Yang, Y.-M. Xie, X.-J. Gao, J. Senior, K. Watanabe, T. Taniguchi, X. Lu, A. P. Higginbotham, K. T. Law, and D. K. Efetov, Symmetry-broken Josephson junctions and superconducting diodes in magic-angle twisted bilayer graphene, Nat. Commun. **14**, 2396 (2023).
[34] H. Zhou, L. Holleis, Y. Saito, L. Cohen, W. Huynh, C. L. Patterson, F. Yang, T. Taniguchi, K. Watanabe, and A. F. Young, Isospin magnetism and spin-polarized superconductivity in Bernal bilayer graphene, Science **375**, 774 (2022).
[35] S. C. de la Barrera, S. Aronson, Z. Zheng, K. Watanabe, T. Taniguchi, Q. Ma, P. Jarillo-Herrero, and R. Ashoori, Cascade of isospin phase transitions in Bernal-stacked bilayer graphene at zero magnetic field, Nat. Phys. **18**, 771 (2022).
[36] A. M. Seiler, F. R. Geisenhof, F. Winterer, K. Watanabe, T. Taniguchi, T. Xu, F. Zhang, and R. T. Weitz, Quantum cascade of correlated phases in trigonally warped bilayer graphene, Nature (London) **608**, 298 (2022).
[37] Y. Zhang, R. Polski, A. Thomson, É. Lantagne-Hurtubise, C. Lewandowski, H. Zhou, K. Watanabe, T. Taniguchi, J. Alicea, and S. Nadj-Perge, Enhanced superconductivity in spin–orbit proximitized bilayer graphene, Nature (London) **613**, 268 (2023).
[38] L. Holleis, C. L. Patterson, Y. Zhang, H. M. Yoo, H. Zhou, T. Taniguchi, K. Watanabe, S. Nadj-Perge, and A. F. Young, Ising superconductivity and nematicity in Bernal bilayer graphene with strong spin orbit coupling, arXiv:2303.00742.
[39] J.-X. Lin, Y. Wang, N. J. Zhang, K. Watanabe, T. Taniguchi, L. Fu, and J. I. A. Li, Spontaneous momentum polarization and diodicity in Bernal bilayer graphene, arXiv:2302.04261.
[40] H. Zhou, T. Xie, A. Ghazaryan, T. Holder, J. R. Ehrets, E. M. Spanton, T. Taniguchi, K. Watanabe, E. Berg, M.

Serbyn, and A. F. Young, Half- and quarter-metals in rhombohedral trilayer graphene, Nature (London) **598**, 429 (2021).
[41] H. Zhou, T. Xie, T. Taniguchi, K. Watanabe, and A. F. Young, Superconductivity in rhombohedral trilayer graphene, Nature (London) **598**, 434 (2021).
[42] A. Ghazaryan, T. Holder, M. Serbyn, and E. Berg, Unconventional Superconductivity in Systems with Annular Fermi Surfaces: Application to Rhombohedral Trilayer Graphene, Phys. Rev. Lett. **127**, 247001 (2021).
[43] S. Chatterjee, T. Wang, E. Berg, and M. P. Zaletel, Intervalley coherent order and isospin fluctuation mediated superconductivity in rhombohedral trilayer graphene, Nat. Commun. **13**, 6013 (2022).
[44] T. Cea, P. A. Pantaleón, V. o. T. Phong, and F. Guinea, Superconductivity from repulsive interactions in rhombohedral trilayer graphene: A Kohn-Luttinger-like mechanism, Phys. Rev. B **105**, 075432 (2022).
[45] A. L. Szabó and B. Roy, Metals, fractional metals, and superconductivity in rhombohedral trilayer graphene, Phys. Rev. B **105**, L081407 (2022).
[46] Y.-Z. You and A. Vishwanath, Kohn-Luttinger superconductivity and intervalley coherence in rhombohedral trilayer graphene, Phys. Rev. B **105**, 134524 (2022).
[47] Y.-Z. Chou, F. Wu, J. D. Sau, and S. Das Sarma, Acoustic-phonon-mediated superconductivity in moiréless graphene multilayers, Phys. Rev. B **106**, 024507 (2022).
[48] Y.-Z. Chou, F. Wu, and S. Das Sarma, Enhanced superconductivity through virtual tunneling in Bernal bilayer graphene coupled to WSe_2, Phys. Rev. B **106**, L180502 (2022).
[49] A. S. Patri and T. Senthil, Strong correlations in ABC-stacked trilayer graphene: Moiré is important, Phys. Rev. B **107**, 165122 (2023).
[50] J. B. Curtis, N. R. Poniatowski, Y. Xie, A. Yacoby, E. Demler, and P. Narang, Stabilizing Fluctuating Spin-Triplet Superconductivity in Graphene via Induced Spin-Orbit Coupling, Phys. Rev. Lett. **130**, 196001 (2023).
[51] G. Wagner, Y. H. Kwan, N. Bultinck, S. H. Simon, and S. A. Parameswaran, Superconductivity from repulsive interactions in Bernal-stacked bilayer graphene, arXiv:2302.00682.
[52] A. Jimeno-Pozo, H. Sainz-Cruz, T. Cea, P. A. Pantaleón, and F. Guinea, Superconductivity from electronic interactions and spin-orbit enhancement in bilayer and trilayer graphene, Phys. Rev. B **107**, L161106 (2023).
[53] W. Qin, C. Huang, T. Wolf, N. Wei, I. Blinov, and A. H. MacDonald, Functional Renormalization Group Study of Superconductivity in Rhombohedral Trilayer Graphene, Phys. Rev. Lett. **130**, 146001 (2023).
[54] D.-C. Lu, T. Wang, S. Chatterjee, and Y.-Z. You, Correlated metals and unconventional superconductivity in rhombohedral trilayer graphene: A renormalization group analysis, Phys. Rev. B **106**, 155115 (2022).
[55] H. Dai, R. Ma, X. Zhang, T. Guo, and T. Ma, Quantum monte carlo study of superconductivity in rhombohedral trilayer graphene under an electric field, Phys. Rev. B **107**, 245106 (2023).
[56] Z. Dong, A. V. Chubukov, and L. Levitov, Transformer spin-triplet superconductivity at the onset of isospin order in bilayer graphene, Phys. Rev. B **107**, 174512 (2023).
[57] G. Shavit and Y. Oreg, Inducing superconductivity in bilayer graphene by alleviation of the Stoner blockade, Phys. Rev. B **108**, 024510 (2023).
[58] Z. Dong, P. A. Lee, and L. S. Levitov, Signatures of cooper pair dynamics and quantum-critical superconductivity in tunable carrier bands, arXiv:2304.09812.
[59] R. Su, M. Kuiri, K. Watanabe, T. Taniguchi, and J. Folk, Superconductivity in twisted double bilayer graphene stabilized by WSe_2, Nat. Mater. (2023).
[60] M. Xie and S. Das Sarma, Flavor symmetry breaking in spin-orbit coupled bilayer graphene, Phys. Rev. B **107**, L201119 (2023).
[61] F. Pientka, A. Keselman, E. Berg, A. Yacoby, A. Stern, and B. I. Halperin, Topological Superconductivity in a Planar Josephson Junction, Phys. Rev. X **7**, 021032 (2017).
[62] M. Hell, M. Leijnse, and K. Flensberg, Two-Dimensional Platform for Networks of Majorana Bound States, Phys. Rev. Lett. **118**, 107701 (2017).
[63] H. Ren, F. Pientka, S. Hart, A. T. Pierce, M. Kosowsky, L. Lunczer, R. Schlereth, B. Scharf, E. M. Hankiewicz, L. W. Molenkamp, B. I. Halperin, and A. Yacoby, Topological superconductivity in a phase-controlled Josephson junction, Nature (London) **569**, 93 (2019).
[64] A. Fornieri, A. M. Whiticar, F. Setiawan, E. Portolés, A. C. C. Drachmann, A. Keselman, S. Gronin, C. Thomas, T. Wang, R. Kallaher, G. C. Gardner, E. Berg, M. J. Manfra, A. Stern, C. M. Marcus, and F. Nichele, Evidence of topological superconductivity in planar Josephson junctions, Nature (London) **569**, 89 (2019).
[65] C. T. Ke, C. M. Moehle, F. K. de Vries, C. Thomas, S. Metti, C. R. Guinn, R. Kallaher, M. Lodari, G. Scappucci, T. Wang, R. E. Diaz, G. C. Gardner, M. J. Manfra, and S. Goswami, Ballistic superconductivity and tunable π–junctions in InSb quantum wells, Nat. Commun. **10**, 3764 (2019).
[66] M. C. Dartiailh, W. Mayer, J. Yuan, K. S. Wickramasinghe, A. Matos-Abiague, I. Žutić, and J. Shabani, Phase Signature of Topological Transition in Josephson Junctions, Phys. Rev. Lett. **126**, 036802 (2021).
[67] A. Banerjee, O. Lesser, M. A. Rahman, H.-R. Wang, M.-R. Li, A. Kringhøj, A. M. Whiticar, A. C. C. Drachmann, C. Thomas, T. Wang, M. J. Manfra, E. Berg, Y. Oreg, A. Stern, and C. M. Marcus, Signatures of a topological phase transition in a planar Josephson junction, Phys. Rev. B **107**, 245304 (2023).
[68] T. Wang, M. Vila, M. P. Zaletel, and S. Chatterjee, Electrical control of magnetism in spin-orbit coupled graphene multilayers, arXiv:2303.04855.
[69] Y. Zhumagulov, D. Kochan, and J. Fabian, Emergent correlated phases in rhombohedral trilayer graphene induced by proximity spin-orbit and exchange coupling, arXiv:2305.14277.
[70] J. M. Koh, J. Alicea, and Étienne Lantagne-Hurtubise, Correlated phases in spin-orbit-coupled rhombohedral trilayer graphene, arXiv:2306.12486.
[71] N. Bultinck, E. Khalaf, S. Liu, S. Chatterjee, A. Vishwanath, and M. P. Zaletel, Ground State and Hidden Symmetry of Magic-Angle Graphene at Even Integer Filling, Phys. Rev. X **10**, 031034 (2020).

[72] Y. Zhang, K. Jiang, Z. Wang, and F. Zhang, Correlated insulating phases of twisted bilayer graphene at commensurate filling fractions: A Hartree-Fock study, Phys. Rev. B **102**, 035136 (2020).

[73] B. Lian, Z.-D. Song, N. Regnault, D. K. Efetov, A. Yazdani, and B. A. Bernevig, Twisted bilayer graphene. iv. exact insulator ground states and phase diagram, Phys. Rev. B **103**, 205414 (2021).

[74] G. Wagner, Y. H. Kwan, N. Bultinck, S. H. Simon, and S. A. Parameswaran, Global Phase Diagram of the Normal State of Twisted Bilayer Graphene, Phys. Rev. Lett. **128**, 156401 (2022).

[75] T. Wang, D. E. Parker, T. Soejima, J. Hauschild, S. Anand, N. Bultinck, and M. P. Zaletel, Kekulé spiral order in magic-angle graphene: A density matrix renormalization group study, arXiv:2211.02693.

[76] X. Liu, G. Farahi, C.-L. Chiu, Z. Papic, K. Watanabe, T. Taniguchi, M. P. Zaletel, and A. Yazdani, Visualizing broken symmetry and topological defects in a quantum Hall ferromagnet, Science **375**, 321 (2022).

[77] A. Coissard, D. Wander, H. Vignaud, A. G. Grushin, C. Repellin, K. Watanabe, T. Taniguchi, F. Gay, C. B. Winkelmann, H. Courtois, H. Sellier, and B. Sacépé, Imaging tunable quantum Hall broken-symmetry orders in graphene, Nature (London) **605**, 51 (2022).

[78] K. P. Nuckolls, R. L. Lee, M. Oh, D. Wong, T. Soejima, J. P. Hong, D. Călugăru, J. Herzog-Arbeitman, B. A. Bernevig, K. Watanabe, T. Taniguchi, N. Regnault, M. P. Zaletel, and A. Yazdani, Quantum textures of the many-body wavefunctions in magic-angle graphene, Nature (London) **620**, 525 (2023).

[79] H. Kim, Y. Choi, Étienne Lantagne-Hurtubise, C. Lewandowski, A. Thomson, L. Kong, H. Zhou, E. Baum, Y. Zhang, L. Holleis, K. Watanabe, T. Taniguchi, A. F. Young, J. Alicea, and S. Nadj-Perge, Imaging inter-valley coherent order in magic-angle twisted trilayer graphene, arXiv:2304.10586.

[80] B. Nijholt and A. R. Akhmerov, Orbital effect of magnetic field on the Majorana phase diagram, Phys. Rev. B **93**, 235434 (2016).

[81] M. e. Aghaee (Microsoft Quantum Collaboration), InAs-Al hybrid devices passing the topological gap protocol, Phys. Rev. B **107**, 245423 (2023).

[82] See Supplemental Material at http://link.aps.org/supplemental/10.1103/PhysRevLett.131.146601 for details, including: (1) minimal model for BLG at finite displacement fields, (2) spin-orbit coupling in the minimal model, (3) determining the topological region with the scattering matrix method, (4) incorporating nematicity, (5) effective tight-binding Hamiltonian for BLG/WSe_2 Josephson junction, (6) the minimal topological gap in various parameter regions, (7) tunneling spectroscopy and Majorana zero-modes, and (8) computing atomically resolved Majorana zero mode wavefunctions, which includes Refs. [83–94].

[83] J. Jung and A. H. MacDonald, Accurate tight-binding models for the π bands of bilayer graphene, Phys. Rev. B **89**, 035405 (2014).

[84] Z. Wang, D.-K. Ki, J. Y. Khoo, D. Mauro, H. Berger, L. S. Levitov, and A. F. Morpurgo, Origin and Magnitude of 'Designer' Spin-Orbit Interaction in Graphene on Semiconducting Transition Metal Dichalcogenides, Phys. Rev. X **6**, 041020 (2016).

[85] B. Yang, M. Lohmann, D. Barroso, I. Liao, Z. Lin, Y. Liu, L. Bartels, K. Watanabe, T. Taniguchi, and J. Shi, Strong electron-hole symmetric Rashba spin-orbit coupling in graphene/monolayer transition metal dichalcogenide heterostructures, Phys. Rev. B **96**, 041409(R) (2017).

[86] D. Wang, S. Che, G. Cao, R. Lyu, K. Watanabe, T. Taniguchi, C. N. Lau, and M. Bockrath, Quantum Hall effect measurement of spin–orbit coupling strengths in ultraclean bilayer graphene/WSe_2 heterostructures, Nano Lett. **19**, 7028 (2019).

[87] J. Amann, T. Völkl, T. Rockinger, D. Kochan, K. Watanabe, T. Taniguchi, J. Fabian, D. Weiss, and J. Eroms, Counterintuitive gate dependence of weak antilocalization in bilayer graphene/WSe_2 heterostructures, Phys. Rev. B **105**, 115425 (2022).

[88] M. Gmitra, D. Kochan, P. Högl, and J. Fabian, Trivial and inverted Dirac bands and the emergence of quantum spin Hall states in graphene on transition-metal dichalcogenides, Phys. Rev. B **93**, 155104 (2016).

[89] M. Gmitra and J. Fabian, Proximity Effects in Bilayer Graphene on Monolayer WSe_2: Field-Effect Spin Valley Locking, Spin-Orbit Valve, and Spin Transistor, Phys. Rev. Lett. **119**, 146401 (2017).

[90] M. P. Zaletel and J. Y. Khoo, The gate-tunable strong and fragile topology of multilayer-graphene on a transition metal dichalcogenide, arXiv:1901.01294.

[91] C. W. J. Beenakker, Universal Limit of Critical-Current Fluctuations in Mesoscopic Josephson Junctions, Phys. Rev. Lett. **67**, 3836 (1991).

[92] Y.-M. Xie, K. T. Law, and P. A. Lee, Topological superconductivity in EuS/Au/superconductor heterostructures, Phys. Rev. Res. **3**, 043086 (2021).

[93] S. Manna, P. Wei, Y. Xie, K. T. Law, P. A. Lee, and J. S. Moodera, Signature of a pair of Majorana zero modes in superconducting gold surface states, Proc. Natl. Acad. Sci. U.S.A. **117**, 8775 (2020).

[94] J. P. Hong, T. Soejima, and M. P. Zaletel, Detecting Symmetry Breaking in Magic Angle Graphene using Scanning Tunneling Microscopy, Phys. Rev. Lett. **129**, 147001 (2022).

[95] Y. Li and M. Koshino, Twist-angle dependence of the proximity spin-orbit coupling in graphene on transition-metal dichalcogenides, Phys. Rev. B **99**, 075438 (2019).

[96] A. David, P. Rakyta, A. Kormányos, and G. Burkard, Induced spin-orbit coupling in twisted graphene–transition metal dichalcogenide heterobilayers: Twistronics meets spintronics, Phys. Rev. B **100**, 085412 (2019).

[97] T. Naimer, K. Zollner, M. Gmitra, and J. Fabian, Twist-angle dependent proximity induced spin-orbit coupling in graphene/transition metal dichalcogenide heterostructures, Phys. Rev. B **104**, 195156 (2021).

[98] J. O. Island, X. Cui, C. Lewandowski, J. Y. Khoo, E. M. Spanton, H. Zhou, D. Rhodes, J. C. Hone, T. Taniguchi, K. Watanabe, L. S. Levitov, M. P. Zaletel, and A. F. Young, Spin–orbit-driven band inversion in bilayer graphene by the van der Waals proximity effect, Nature (London) **571**, 85 (2019).

[99] J. Jung, M. Polini, and A. H. MacDonald, Persistent current states in bilayer graphene, Phys. Rev. B **91**, 155423 (2015).

[100] Z. Dong, M. Davydova, O. Ogunnaike, and L. Levitov, Isospin- and momentum-polarized orders in bilayer graphene, Phys. Rev. B **107**, 075108 (2023).

[101] J. Liu, A. C. Potter, K. T. Law, and P. A. Lee, Zero-Bias Peaks in the Tunneling Conductance of Spin-Orbit-Coupled Superconducting Wires with and without Majorana End-States, Phys. Rev. Lett. **109**, 267002 (2012).

[102] D. Bagrets and A. Altland, Class *d* Spectral Peak in Majorana Quantum Wires, Phys. Rev. Lett. **109**, 227005 (2012).

[103] S. Das Sarma and H. Pan, Disorder-induced zero-bias peaks in Majorana nanowires, Phys. Rev. B **103**, 195158 (2021).

[104] C. Moore, T. D. Stanescu, and S. Tewari, Two-terminal charge tunneling: Disentangling Majorana zero modes from partially separated Andreev bound states in semiconductor-superconductor heterostructures, Phys. Rev. B **97**, 165302 (2018).

[105] J. Chen, B. D. Woods, P. Yu, M. Hocevar, D. Car, S. R. Plissard, E. P. A. M. Bakkers, T. D. Stanescu, and S. M. Frolov, Ubiquitous Non-Majorana Zero-Bias Conductance Peaks in Nanowire Devices, Phys. Rev. Lett. **123**, 107703 (2019).

[106] T. D. Stanescu and S. Tewari, Robust low-energy Andreev bound states in semiconductor-superconductor structures: Importance of partial separation of component Majorana bound states, Phys. Rev. B **100**, 155429 (2019).

[107] E. Prada, P. San-Jose, M. W. A. de Moor, A. Geresdi, E. J. H. Lee, J. Klinovaja, D. Loss, J. Nygård, R. Aguado, and L. P. Kouwenhoven, From Andreev to Majorana bound states in hybrid superconductor–semiconductor nanowires, Nat. Rev. Phys. **2**, 575 (2020).

[108] A. Haim and A. Stern, Benefits of Weak Disorder in One-Dimensional Topological Superconductors, Phys. Rev. Lett. **122**, 126801 (2019).

[109] T. Laeven, B. Nijholt, M. Wimmer, and A. R. Akhmerov, Enhanced Proximity Effect in Zigzag-Shaped Majorana Josephson Junctions, Phys. Rev. Lett. **125**, 086802 (2020).

[110] Y.-M. Xie, D. K. Efetov, and K. T. Law, φ_0-josephson junction in twisted bilayer graphene induced by a valley-polarized state, Phys. Rev. Res. **5**, 023029 (2023).

[111] J.-X. Hu, Z.-T. Sun, Y.-M. Xie, and K. T. Law, Josephson Diode Effect Induced by Valley Polarization in Twisted Bilayer Graphene, Phys. Rev. Lett. **130**, 266003 (2023).

[112] H. Sainz-Cruz, P. A. Pantaleón, V. o. T. Phong, A. Jimeno-Pozo, and F. Guinea, Junctions and Superconducting Symmetry in Twisted Bilayer Graphene, Phys. Rev. Lett. **131**, 016003 (2023).

[113] A. Uri, S. Grover, Y. Cao, J. A. Crosse, K. Bagani, D. Rodan-Legrain, Y. Myasoedov, K. Watanabe, T. Taniguchi, P. Moon, M. Koshino, P. Jarillo-Herrero, and E. Zeldov, Mapping the twist-angle disorder and Landau levels in magic-angle graphene, Nature (London) **581**, 47 (2020).

[114] J. H. Wilson, Y. Fu, S. Das Sarma, and J. H. Pixley, Disorder in twisted bilayer graphene, Phys. Rev. Res. **2**, 023325 (2020).